EBioMedicine 27 (2018) 176–181

Contents lists available at ScienceDirect

EBioMedicine

journal homepage: www.ebiomedicine.com

Research Paper

Meningioma growth dynamics assessed by radiocarbon retrospective birth dating

Hagen B. Huttner [a,b,1], Olaf Bergmann [a,c,1], Mehran Salehpour [d], Raouf El Cheikh [e], Makoto Nakamura [f], Angelo Tortora [f], Paula Heinke [c], Roland Coras [g], Elisabet Englund [h], Ilker Y. Eyüpoglu [i], Joji B. Kuramatsu [b], Sebastian S. Roeder [b], Stephan P. Kloska [j], Iris Muehlen [j], Arnd Doerfler [j], Stefan Schwab [b], Göran Possnert [d], Samuel Bernard [k], Jonas Frisén [a,*]

[a] Department of Cell and Molecular Biology, Karolinska Institute, Sweden
[b] Department of Neurology, University Hospital Erlangen, Germany
[c] DFG-Center for Regenerative Therapies Dresden, Technische Universität Dresden, Dresden, Germany
[d] Division of Ion Physics, Department of Physics and Astronomy, Uppsala University, Sweden
[e] Aix Marseille University, Inserm S 911 CRO2, SMARTc Pharmacokinetics Unit, Marseille, France
[f] Department of Neurosurgery, University Hospital Hannover, Germany
[g] Department of Neuropathology, University Hospital Erlangen, Germany
[h] Department of Pathology, University Hospital Lund, Sweden
[i] Department of Neurosurgery, University Hospital Erlangen, Germany
[j] Department of Neuroradiology, University Hospital Erlangen, Germany
[k] Institut Camille Jordan, CNRS UMR 5208, University of Lyon, Villeurbanne, France

ARTICLE INFO

Article history:
Received 1 August 2017
Received in revised form 15 December 2017
Accepted 15 December 2017
Available online 19 December 2017

Keywords:
Radiocarbon
C14
Meningioma
Tumor growth

ABSTRACT

It is not known how long it takes from the initial neoplastic transformation of a cell to the detection of a tumor, which would be valuable for understanding tumor growth dynamics. Meningiomas show a broad histological, genetic and clinical spectrum, are usually benign and considered slowly growing. There is an intense debate regarding their age and growth pattern and when meningiomas should be resected. We have assessed the age and growth dynamics of 14 patients with meningiomas (WHO grade I: n = 6 with meningothelial and n = 6 with fibrous subtype, as well as n = 2 atypical WHO grade II meningiomas) by combining retrospective birth-dating of cells by analyzing incorporation of nuclear-bomb-test-derived ^{14}C, analysis of cell proliferation, cell density, MRI imaging and mathematical modeling. We provide an integrated model of the growth dynamics of benign meningiomas. The mean age of WHO grade I meningiomas was 22.1 ± 6.5 years, whereas atypical WHO grade II meningiomas originated 1.5 ± 0.1 years prior to surgery ($p < 0.01$). We conclude that WHO grade I meningiomas are very slowly growing brain tumors, which are resected in average two decades after time of origination.

1. Introduction

It is not known how long it takes from the initial neoplastic transformation of a cell to the detection of a tumor, which would be valuable for understanding tumor growth dynamics and to establish at what stage therapy may be needed. Along with gliomas, meningiomas are the most frequent CNS tumors with an annual incidence of about 4–5/100.000 individuals (Wiemels et al., 2010; Whittle et al., 2004). Meningiomas arise from arachnoidal cap cells and show a broad histological, genetical and clinicopathological spectrum (Riemenschneider et al., 2006). The dignity of the various subtypes is graded according to the World Health Organization (WHO) classification, the vast majority of meningiomas (~80%) being benign, slowly growing, WHO grade I tumors (Louis et al., 2016; Riemenschneider et al., 2006). There has been an intensive debate regarding the age of meningiomas (Braunstein and Vick, 1997; Herscovici et al., 2004; Nakasu et al., 2011). Estimates were often based on consecutive MRI imaging of patients with incidental and recurrent meninigiomas (Nakasu et al., 2011; Nakamura et al., 2003; Herscovici et al., 2004; Nakamura et al., 2005). However, it has been difficult to establish their growth pattern and to decide when meningiomas should be resected (Braunstein and Vick, 1997; Herscovici et al., 2004; Nakasu et al., 2011).

We used retrospective birth dating (Spalding et al., 2005) to assess the age of meningioma cells. This strategy takes advantage of the dramatically elevated levels of the isotope ^{14}C caused by above ground

* Corresponding author at: Karolinska Institute, Department of Cell and Molecular Biology, SE-171 77 Stockholm, Sweden.
E-mail address: jonas.frisen@ki.se (J. Frisén).
[1] These two authors contributed equally

https://doi.org/10.1016/j.ebiom.2017.12.020

nuclear bomb testing during the Cold War (De Vries, 1958; Nydal and Lövseth, 1965; Levin and Kromer, 2004). ^{14}C together with oxygen forms $^{14}CO_2$ and enters the food chain through plant photosynthesis such that the ^{14}C concentration in the human body closely corresponds to that in the atmosphere at any given time (Libby et al., 1964; Harkness, 1972). During cell division ^{14}C is integrated into genomic DNA, resulting in a stable date mark (Spalding et al., 2005). We have previously used this technique to establish the age and cell renewal rates of various human cell types including neurons, oligodendrocytes, heart muscle and fat cells (Bergmann et al., 2009; Huttner et al., 2014; Yeung et al., 2014; Bergmann et al., 2015b; Bergmann et al., 2015a; Spalding et al., 2013; Spalding et al., 2008).

We have assessed the age and growth dynamics of meningiomas by combining ^{14}C-based retrospective birth dating, analysis of cell proliferation, cell density, MRI imaging and mathematical modeling. We provide an integrated model of the growth dynamics of benign meningioma and show that growth curve estimation models may benefit from incorporating ^{14}C data to predict future progress and facilitate the decision of whether to remove a detected meningioma.

2. Material and Methods

2.1. Patient Selection and Tumor Sample Preparation

All investigated samples were taken from tumor tissue bio-banks of the Departments of Neurosurgery of the University Hospitals Hannover and Erlangen, Germany. Upon meningioma surgery routine sample handling included (i) instantaneous section analysis, (ii) paraffin embedding of the gross of the sample for subsequent neuropathological characterization as well as (iii) snap freezing a representative tumor part (roughly 0.5 × 0.5 × 0.5 cm) and unfixed storage of this tumor aliquot at −80 °C immediately after surgery. All subjects gave written informed consent and the study was approved the local institutional review boards (Ethics Committee Approval No: 104_13B).

2.2. Clinical Characteristics and Imaging

Demographic and baseline clinical information were collected by screening the institutional electronic databases and by reviewing the patients´ medical charts. All patients underwent MR imaging and examinations were reviewed on a PACS workstation using FDA-approved software (syngo.via, MR Onco Brain, Siemens, Erlangen, Germany). Evaluation of each examination was performed on contrast-enhanced T1-weighted images with a slice thickness of 5 mm or less. For volume measurement, the semi-automated lesion segmentation of the software based on signal intensity values was used. The appropriate lesion detection was approved by two neuroradiologists in consensus and the volume was calculated by the software for each examination and time point.

2.3. Histology and Immunohistochemistry

Initial histological analysis for verification of tumor type and WHO classification (Louis et al., 2016) was performed by local experienced neuropathologists on formalin embedded tissue pieces (frozen tumor tissue samples, 20 μm microtome sectioning and fixed in 4% formaldehyde buffered in PBS for 30 min). Standard HE staining confirmed meningothelial and fibrous/fibromatous tumor types. Sections were incubated with the primary antibody overnight at 4 °C: mouse Ki-67 (Mib1 monoclonal, 1:200, Thermo Fischer Scientific), phospho-Histone H3 (rabbit, Abcam, 1:1000) and visualized with the matching secondary antibody conjugated to Alexa 488, 546 or 647 (Invitrogen, 1:500). Apoptosis was detected with TUNEL staining (Click-It Alexa-Flour, Invitrogen). The indices for positive cells labeled with, Ki-67, phospho-Histone H3 (p-HH3), and TUNEL respectively, were calculated referring to overall DAPI-positive nuclei and averaged on 5 arbitrarily chosen high power fields (400× magnification) (Riemenschneider et al., 2006; Vranic et al., 2010; Louis et al., 2016). Immunohistochemistry was analyzed using a confocal microscope (LSM 710, Carl Zeiss Jena, Germany using ZEN software).

2.4. Isolation of Nuclei

Tumor tissue samples were thawed at room temperature and homogenized in 10 ml lysis buffer (0.32 M sucrose, 5 mM $CaCl_2$, 3 mM magnesium acetate, 0.1 mM EDTA, 10 mM Tris-HCl [pH 8.0] and 1 mM DTT) using a T25-digital-Ultra-Turrax® disperser (www.ika.com). Samples were then diluted with additional 190 ml lysis buffer, dounce homogenized, filtered twice in 100 μm and 60 μm Nylon Net Filters (Millipore), equally distributed into 4 tubes with 50 ml and subsequently centrifuged (700 ×*g* for 10 min at 4 °C). The pellets of each of the four tubes were resuspended in 2.5 ml lysis buffer, pooled and added to 20 ml of sucrose solution (1.7 M sucrose, 3 mM magnesium acetate, 1 mM DTT, and 10 mM Tris-HCl [pH 8.0]). As described previously (Bergmann et al., 2012; Huttner et al., 2014), the samples were subjected to a gradient centrifugation after layered onto a cushion of 10 ml sucrose solution (36,500 ×*g* for 2.20 h at 4 °C). The isolated nuclei were resuspended in 10 ml nuclei storage buffer (NSB; 10 mM Tris [pH 7.2], 2 mM $MgCl_2$, 70 mM KCl, and 15% sucrose) and again centrifuged for 10 min at 700 x g at 4 °C. The resulting pellet was transferred to glassware for consecutive DNA extraction.

2.5. Extraction of DNA

As published earlier (Bergmann et al., 2012; Huttner et al., 2014), DNA extraction experiments were carried out in a clean room (ISO8) to prevent any carbon contamination. All used instruments and glassware were prebaked at 450 °C for 4 h. DNA isolation was performed according to (Bergmann et al., 2012, Huttner et al., 2014); briefly summarized here: to each sample of collected nuclei 500 μl of DNA lysis buffer (100 mM Tris [pH 8.0], 200 mM NaCl, 1% SDS, and 5 mM EDTA) and 6 μl Proteinase K (20 mg/ml) were added and incubated overnight at 65 °C. Three μl RNase cocktail (Ambion) was added and incubated at 65 °C for 45 min. We added half of the existing volume of 5 M NaCl solution, vortexed for 15 s and the solution was centrifuged for 3 min at 13,000 rpm for 3 min. The supernatant containing the DNA was transferred to a 12 ml glass vial. Three times the volume of absolute ethanol was added, and the glass vial was inverted several times to precipitate the DNA. The DNA precipitate was washed three times in DNA washing solution (70% Ethanol [v/v] and 0.5 M NaCl) and dried out overnight at 65 °C. Finally, 500 μl DNase/RNAase free water (GIBCO/Invitrogen) was added to the glassware allowing the crystallized DNA to be dissolved entirely during another 24 h incubation at 65 °C. The DNA was quantified and DNA purity verified by UV spectroscopy (NanoDrop).

2.6. Accelerator Mass Spectrometry (AMS)

As described previously, all AMS analyses were performed blind to age and clinical information (Huttner et al., 2014). Purified DNA samples suspended in water were combusted to CO_2, and reduced to graphite according to the procedures described previously (Spalding et al., 2013). ^{14}C AMS measurements of graphitized samples were carried out at the Tandem Accelerator Laboratory in Uppsala, Sweden using a 5 MV Pelletron tandem accelerator. ^{14}C measurement results and carbon background subtraction are reported as described earlier (Spalding et al., 2013; Salehpour et al., 2013; Salehpour et al., 2015). Age calibration of ^{14}C concentrations was performed using the software CALIbomb (http://calib.qub.ac.uk/CALIBomb) with the following parameters: smoothing in years, 1 year; resolution, 0.2; ^{14}C calibration, two sigma.

2.7. Interpretation of ^{14}C Analysis and Mathematical Modeling of Growth Dynamics

To estimate the age of the tumor in each patient a mathematical model was established that described the proliferation and aging of a given cell population. According to the Gompertz law, the tumor size follows a sigmoid curve: growth is initially exponential and slows down as the tumor size approaches a maximal value. The Gompertz law was shown to reproduce well the growth dynamics in low grade meningiomas (Nakamura et al., 2003). During growth the age of tumor cells is tracked by the age-structure of the equation (see supplementary methods for details). We assumed that newborn cells were aged zero and that mother cells retained their age at division. Estimates were based on two experimentally measured quantities for each patient: the tumor volume (one or two time points) and the average age of the tumor cells. Using the model and available neuropathological data, we estimated the values of three parameters for each patient: a proliferation coefficient describing how fast the tumor grows initially, a carrying capacity describing the maximal size the tumor can take, and the time since the beginning of tumor development (the time since the tumor had a volume corresponding to one cell). For patients with only one tumor volume measurement, the model was complemented with published tumor volume growth data (Nakamura et al., 2003). For each patient, the parameters were estimated using a least-square method that minimizes the difference between the observations and the model predictions (Sen and Srivastava, 1990).

3. Results

3.1. ^{14}C-based Retrospective Birth Dating Determines the Average Age of Meningioma Cells

We included a total of 14 patients with surgically resected meningiomas in the study (supplementary Table 1), including benign World Health Organization (WHO) grade I (meningothelial, n = 6, and fibrous, n = 6) and atypical WHO grade II (n = 2) tumors. Five patients with meningiomas were monitored by serial MR imaging and underwent surgery motivated by evidence of tumor growth. The remaining 9 patients were de-novo diagnosed meningioma patients who were clinically symptomatic and were subjected only once to MR imaging prior to surgery.

We measured the average genomic ^{14}C concentrations of all cells constituting the meningioma by accelerator mass spectrometry (Fig. 1A-C). The period between time of surgery and measured averaged ^{14}C–cell-age of each meningioma is shown in Fig. 1D. The average age of all cells within WHO grade I meningiomas dated back 2.3–9.5 years prior to surgery providing evidence of a moderate tumor cell turnover. In contrast, the ^{14}C concentration of the WHO grade II meningiomas closely corresponded to the atmospheric ^{14}C levels of the calendar years of surgery, indicating a high cell turnover. Genomic ^{14}C concentrations of cortical and cerebellar neurons of individuals who did not undergo meningioma surgery but who were born in similar years to the respective meningioma patients were not different from atmospheric ^{14}C values at birth demonstrating no postnatal cellular turnover of

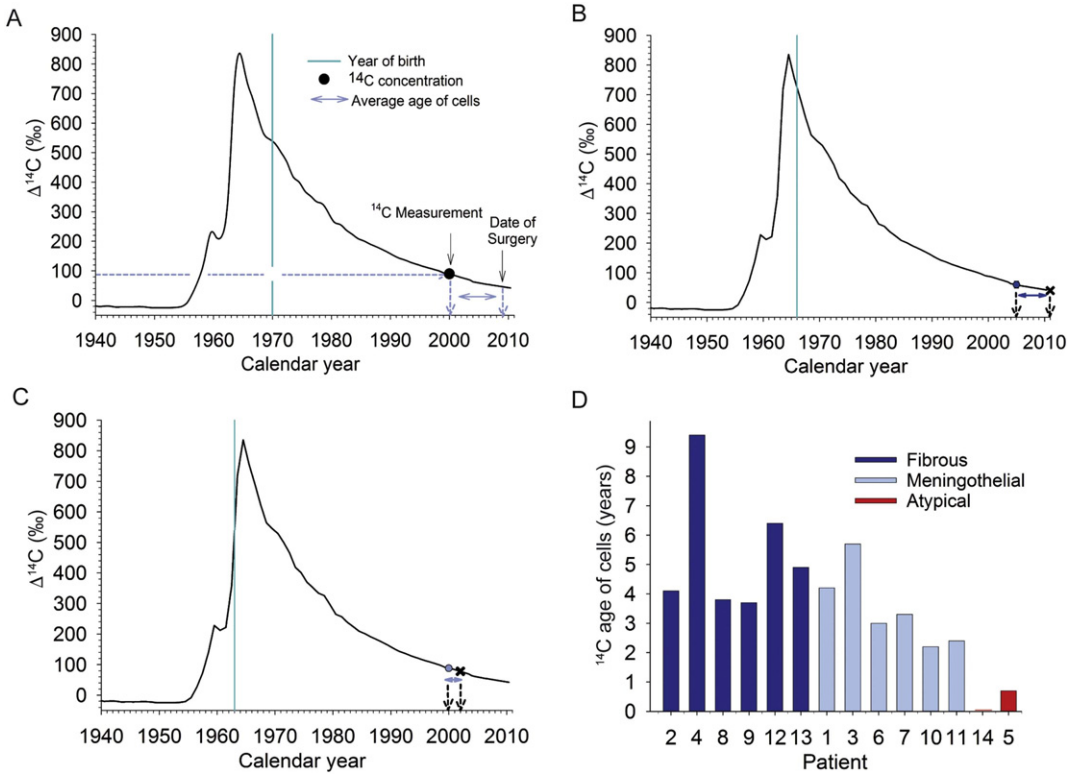

Fig. 1. Retrospective ^{14}C birth-dating to determine the average age of meningioma cells. (A) Schematic presentation of ^{14}C data points of meningiomas. The black curve indicates atmospheric ^{14}C concentrations measured over the last decades in the northern hemisphere. The peak indicates the steep increase in atmospheric ^{14}C levels caused by the above-ground nuclear bomb testing during the Cold War (1950's to 1960's), which declined since the Test Ban Treaty in year 1963. The vertical turquoise line depicts the date of birth of a hypothetical patient. The black dot represents the average hypothetical genomic ^{14}C concentration of all meningioma cells obtained at the time of surgery. The average age of meningioma cells can be established by matching the genomic ^{14}C concentration with atmospheric ^{14}C values (dashed blue lines). The blue arrows indicate the average age of the meningioma cells. (B and C) Examples of a ^{14}C dated fibrous meningioma (case 12) (B), and of meningothelial meningioma (case 11). (D) The average age of meningioma cells (n = 14) at the time of surgery. Note the young ages of atypical WHO grade II meningiomas (red) in comparison to benign meningiomas (blue). Dark blue bars indicate fibrous meningiomas, light blue bars indicate meningothelial meningiomas.

these populations (supplementary Fig. 1) (Bergmann et al., 2012; Huttner et al., 2014).

3.2. Mathematical Modeling to Explore Meningioma Growth Dynamics

To gain further information about the proliferation kinetics, we determined the proportion of cells in cycle by Ki-67 labelling, and of mitotic cells by phospho-Histone H3 (p-HH3) labeling. This revealed a range of Ki-67 frequency between 0.3% and 2.4%, and of p-HH3 frequency between 0.002% and 0.1% in WHO grade I. WHO grade II tumors showed higher frequencies of Ki-67 between 7.1% and 12%, and p-HH3 between 0.4% and 0.8%. In line with the pathological definition of low-grade meningiomas (Riemenschneider et al., 2006), we did not find any evidence for apoptosis (data not shown). The mean tumor cell density in WHO grade I tumors was 5900 ± 750 l/mm^3 and ranged between 3700 and 4900 l/mm^3 in atypical WHO grade II tumors. In addition, when comparing the cell density in meningothelial versus fibrous subtypes we did not observe any significant difference (meningothelial: 5560 ± 437 l/mm^3 vs. fibrous: 6001 ± 101 l/mm^3; p = 0.611).

Retrospective ^{14}C dating allowed establishing the average age of all cells within the meningioma (Fig. 1). Due to tumor expansion the average cell age, however, does not reflect the beginning of meningioma growth, but only the age of the cells present at the time of analysis. To estimate the time of the initial cell transformation and onset of the meningioma in each patient, we applied a mathematical model consisting of an age-structured partial differential equation with Gompertz growth that tracks both the tumor size and the age of the cells (see Supplementary methods for details). The model included the measured ^{14}C data, the cell density and MRI volume measurements (5 patients with follow-up MR imaging, Figs. 2, and 9 patients with one MR imaging prior to surgery, Supplementary Fig. 2).

We predicted future growth dynamics of benign meningiomas by extrapolating the respective Gompertz growth function derived from the age-structured mathematical model (Fig. 3). According to our model 3 of 14 meningiomas were still in pre-exponential growth (lag phase) without having reached exponential growth at the time of surgery (Fig. 3A). Most meningiomas were in the exponential growth phase (n = 6) (Fig. 3B), and three already exited the exponential growth and started to plateau at the time of surgery (Fig. 3C).

3.3. The Onset of Meningioma Growth

The mathematical model allowed calculating the onset of meningioma growth, i.e. the time-point of the first meningioma cell origination (Fig. 4). The mean age of WHO grade I meningiomas was 22.1 ± 6.5 SD years (ranging from 10.8–31.1 years), whereas atypical WHO grade II meningiomas originated 1.5 ± 0.1 SD years prior to surgery (*t*-test: p < 0.001) (Fig. 4A). There was no difference when comparing patients with symptomatic or asymptomatic meningiomas (symptomatic: 23.9 ± 5.1 SD years versus 18.3 ± 8.2 SD years in asymptomatic; t-test: p = 0.174). We observed a statistically significant difference in the age of meningiomas between patients with meningothelial versus fibrous meningioma (meningothelial: 17.8 ± 5.8 SD years versus 26.3 ± SD 4.0 years in fibrous meningiomas; t-test: p = 0.015; Fig. 4B). Given the fact that (i) meningioma volumes at time of surgery were not different (meningothelial: 28.4 (IQR: 2.7–82.7) cm^3 cc versus 29.8 (IQR: 6.3–57.5) cm^3 in fibrous meningiomas; p = 0.936), and (ii) there was no significant difference in proliferation rates (Supplementary table 1), we conclude that fibrous meningiomas have slower growth rates compared to meningothelial variants. Overall, there were no significant correlations of meningioma age with age of patients (R = 0.17; p = 0.61), Ki-67 frequency (R = 0.03; p = 0.92) and p-HH3 frequency (R = 0.10; p = 0.81; Supplementary Fig. 3).

4. Discussion

In contrast to traditional strategies to predict the growth of meningiomas by volumetric measurements (Nakamura et al., 2003; Nakamura et al., 2005; Nakasu et al., 2011), we used ^{14}C birth dating to determine the age of meningioma cells and to investigate growth dynamics of meningiomas. We devised an age-structured mathematical model based on cell age and meningioma growth to predict the time of tumor initiation and thereby the formation age of meningiomas. We demonstrate that the average age of meningioma cells was significantly older in benign compared to atypical meningiomas, and mathematical modeling revealed tumor initiation to date back up to three decades in benign tumors, whereas it was less than two years in their atypical counterparts.

Ki-67 labeling has been used as a parameter to distinguish benign from atypical meningiomas and correlates with the doubling time of benign meningiomas (Roser et al., 2004). Additionally, the mitotic index measured by p-HH3 labeling was reported as an independent predicator of recurrence-free survival in meningioma patients (Olar et al., 2015). However, Ki-67 and mitotic makers provide only a glimpse of the number of proliferating cells at the time of surgery, and Ki-67 and p-HH3 based estimates of turnover dynamics can be biased by focal heterogeneity in cell proliferation (Siegers et al., 1989). Accordingly, we did not find any correlation between Ki-67 and p-HH3 based indices and the age of benign meningiomas. In contrast, ^{14}C birth dating in combination with mathematical modeling allowed establishing age distributions of cell populations present in meningiomas at the time of surgery. We found that the WHO grade I fibrous subtype is older than the meningothelial type, which implies that fibrous subtype is diagnosed later in patients with benign meningiomas. In line with this finding, 50% of all meningothelial meningiomas (3 out of 6) compared to fibrous meningiomas (0 out of 6) became already symptomatic before they reached the exponential growth phase. However, our patient population is not large enough to explicitly answer the question whether meningothelial meningiomas become symptomatic earlier than fibrous tumors e.g. because of subtype characteristics. Another explanation could refer to the different localizations in the brain, with fibrous

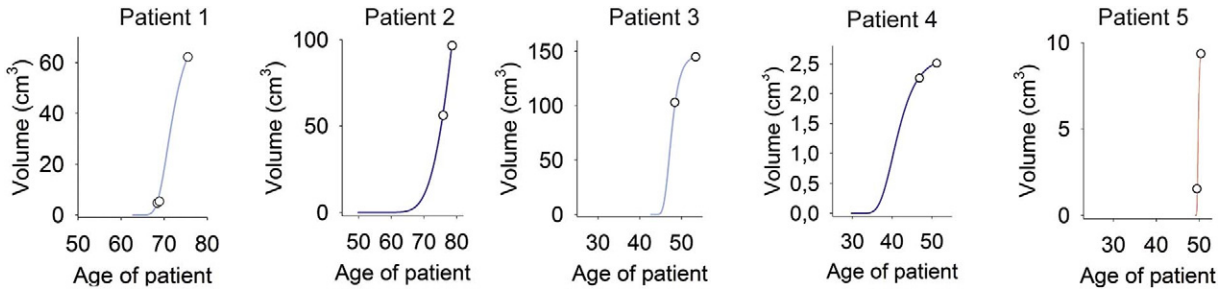

Fig. 2. Growth curves of meningiomas. Model-fitted meningioma growth curves given for 5 patients with benign meningothelial (A and C, light blue), fibrous (B and D, dark blue) and atypical meningiomas (E, red). The growth curves were estimated using nonlinear least-square with uniform weighting. Parameters were based on ^{14}C measurements, histological data and on sequential MRI volumetric measurements (see Methods).

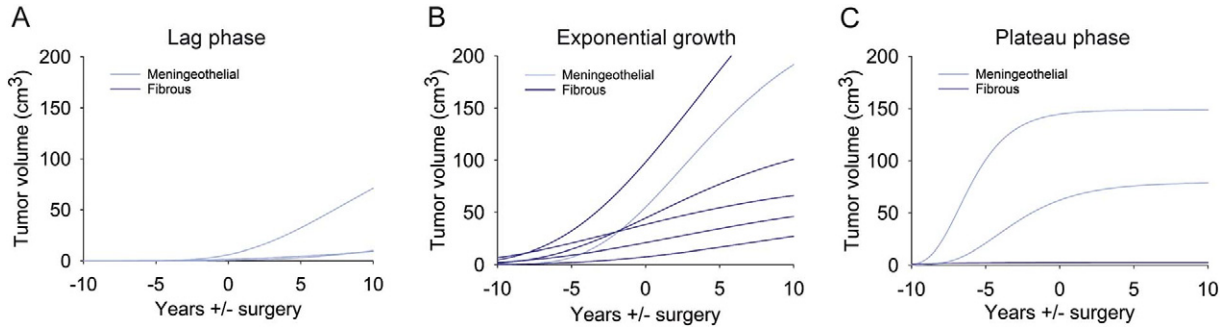

Fig. 3. Growths projection of benign meningiomas. Model-fitted future projections on meningioma growth based on the growth phase at the time of surgery. The Gompertz growth curve can be parted into a lag phase, an exponential growth phase and a plateau phase. (A) Three tumors were surgically removed before reaching the exponential growth phase (lag phase), (B) six tumors were removed being in exponential growth phase, (C) and three tumors already left exponential growth (plateau phase). Dark blue indicates fibrous meningiomas, light blue indicates meningothelial meningiomas. Zero indicates the time of surgery, negative number range (years) indicates growth until surgery, and positive number range (years) indicates growth prediction.

meningiomas occurring rather at the convexity of the scull (Louis et al., 2016). However, in our cohort of patients we did not observe significant differences with respect to meningioma location among meningothelial and fibrous subtypes (supplementary table 1).

Our data suggests that tumor origination occurs throughout life, which is in contrast to the hypothesis that meningiomas are initiated already early in life or in development as suggest by a mouse model based on a biallelic gene inactivation of neurofibromatosis 2 gene (Nf2) in leptomeningeal cells (Kalamarides et al., 2011). Although Nf2 gene inactivation can be found in 50–80% of sporadic meningiomas in humans (Gutmann et al., 1997), our data indicate that tumor origination is not resticted to a critical time window (patient age of tumor origination: range 12 to 62 years of age).

There are several shortcomings, notably the retrospective study design. A larger cohort of patients, preferably enrolled prospectively, would have allowed a more precise subgroup analysis. In addition, we did not obtain control meningeal tissue for ethical reasons why a correlation of the age of meningioma cells with normal meningeal cells was not performed. Further, as this investigation lacked longitudinal prospective follow up information, we could not correlate our findings (i) with clinical end-points such as progression-free survival or functional outcomes, or (ii) possible MRI-based tumor relapse or regrowth. Also, we did not specifically perform molecular profiling, exome sequencing or methylation analyses of the analyzed tissue samples leaving room for uncertainties regarding subtype analysis.

To guide clinical decision making, establishing growth dynamics and answering the question since when benign meningiomas have been growing in individual subjects may help screening and monitoring and may guide diagnostic and therapeutic procedures after biopsy. Specifically, estimates of meningioma growth were often based on consecutive MRI imaging of patients with incidental and recurrent meningiomas (Nakasu et al., 2011; Nakamura et al., 2003; Herscovici et al., 2004; Nakamura et al., 2005). Although this may provide precise information regarding the volume increase of the meningioma during the study period, it is not possible to predict the future growth rate, as the volume expansion goes through different phases. Hence, in clinical routine, there are frequently situations in which a meningioma is diagnosed in an eloquent brain area, or in a surgically only very difficultly accessible tumor site, e.g. immuring vital vessels. While in these patients a meningioma resection may potentially be harmful with possible complications outweighing the benefits of removal, a stereotactical biopsy with subsequent ^{14}C analysis may help predict future growth dynamics and may guide clinical decision making. In this regard it seems valuable to prospectively verify if tumor growth estimations – based on more than two MRI, taking histological aspects into account and including ^{14}C data upon biopsy – may identify such meningiomas that switch from lag phase to exponential growth, and from exponential towards a plateauing growth curve respectively, and which therefore should or not necessarily be resected.

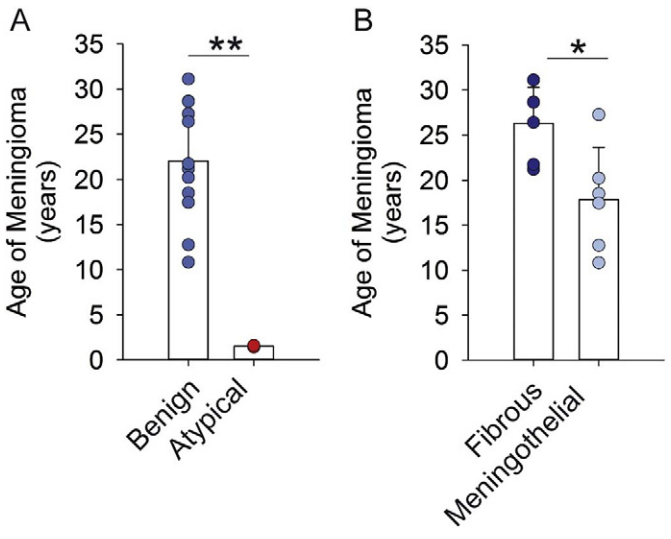

Fig. 4. The age of meningiomas. Mathematical modeling established the age of benign (n = 12), and atypical (n = 2, red) meningiomas. Benign meningiomas were 22 ± 6.5 SD years of age, whereas atypical meningiomas were 1.5 ± 0.1 SD years of age. Benign fibrous meningiomas (n = 6) were 8.5 years older than menigothelial meningiomas (n = 6) at the time of surgery (*t*-test,* $p < 0.05$, **$p < 0.001$).

Acknowledgements and Funding Sources

The study was supported by the Swedish Research Council, The Swedish Cancer Foundation, Tobias Stiftelsen, SSF, Knut och Alice Wallenbergs Stiftelse, the ERC, Ragnar Söderberg Foundation, Åke Wiberg Foundation and Jeanssons Foundations. H.B.H. was supported by research grants of the German DFG (Deutsche Forschungsgemeinschaft, HU1961/1-1 and HU1961/2-1). No funding bodies had any role in study design, data collection and analysis, decision to publish, or preparation of the manuscript.

Conflict of Interest

The authors have declared that no competing interests exist.

Author Contributions

H.B.H., O.B. and J.F. designed the study and wrote the manuscript. H.B.H. and O.B. performed the experiments. M.S. and G.P. performed accelerator mass spectrometry analysis. M.N., A.T., R.C., E.E., I.Y.E., J.B.K.,

P·H, S.R. and S.S. obtained clinical information, provided tissue samples and performed immunohistological analyses. S.P.K. I.M., and A.D analyzed MR images. R.E.C. and S.B. performed statistical analyses and mathematical modeling. All authors critically reviewed the manuscript and approved its final version.

Appendix A. Supplementary data

Supplementary data to this article can be found online at https://doi.org/10.1016/j.ebiom.2017.12.020.

References

Bergmann, O., Bhardwaj, R.D., Bernard, S., Zdunek, S., Barnabe-Heider, F., Walsh, S., Zupicich, J., Alkass, K., Buchholz, B.A., Druid, H., Jovinge, S., Frisen, J., 2009. Evidence for cardiomyocyte renewal in humans. Science 324, 98–102.

Bergmann, O., Liebl, J., Bernard, S., Alkass, K., Yeung, M.S., Steier, P., Kutschera, W., Johnson, L., Landen, M., Druid, H., Spalding, K.L., Frisen, J., 2012. The age of olfactory bulb neurons in humans. Neuron 74, 634–639.

Bergmann, O., Spalding, K.L., Frisen, J., 2015a. Adult neurogenesis in humans. Cold Spring Harb. Perspect. Biol. 7, a018994.

Bergmann, O., Zdunek, S., Felker, A., Salehpour, M., Alkass, K., Bernard, S., Sjostrom, S.L., Szewczykowska, M., Jackowska, T., DOS Remedios, C., Malm, T., Andra, M., Jashari, R., Nyengaard, J.R., Possnert, G., Jovinge, S., Druid, H., Frisen, J., 2015b. Dynamics of cell generation and turnover in the human heart. Cell 161, 1566–1575.

Braunstein, J.B., Vick, N.A., 1997. Meningiomas: the decision not to operate. Neurology 48, 1459–1462.

De Vries, H., 1958. Atomic bomb effect: variation of radiocarbon in plants, shells, and snails in the past 4 years. Science 128, 250–251.

Gutmann, D.H., Giordano, M.J., Fishback, A.S., Guha, A., 1997. Loss of merlin expression in sporadic meningiomas, ependymomas and schwannomas. Neurology 49, 267–270.

Harkness, D.D., 1972. Further investigations of the transfer of bomb 14 C to man. Nature 240, 302–303.

Herscovici, Z., Rappaport, Z., Sulkes, J., Danaila, L., Rubin, G., 2004. Natural history of conservatively treated meningiomas. Neurology 63, 1133–1134.

Huttner, H.B., Bergmann, O., Salehpour, M., Racz, A., Tatarishvili, J., Lindgren, E., Csonka, T., Csiba, L., Hortobagyi, T., Mehes, G., Englund, E., Solnestam, B.W., Zdunek, S., Scharenberg, C., Strom, L., Stahl, P., Sigurgeirsson, B., Dahl, A., Schwab, S., Possnert, G., Bernard, S., Kokaia, Z., Lindvall, O., Lundeberg, J., Frisen, J., 2014. The age and genomic integrity of neurons after cortical stroke in humans. Nat. Neurosci. 17, 801–803.

Kalamarides, M., Stemmer-Rachamimov, A.O., Niwa-Kawakita, M., Chareyre, F., Taranchon, E., Han, Z.Y., Martinelli, C., Lusis, E.A., Hegedus, B., Gutmann, D.H., Giovannini, M., 2011. Identification of a progenitor cell of origin capable of generating diverse meningioma histological subtypes. Oncogene 30, 2333–2344.

Levin, I., Kromer, B., 2004. The tropospheric $^{14}CO_2$ level in mid-latitudes of the northern hemisphere (1959–2003). Radiocarbon 46, 1261–1272.

Libby, W.F., Berger, R., Mead, J.F., Alexander, G.V., Ross, J.F., 1964. Replacement rates for human tissue from atmospheric radiocarbon. Science 146, 1170–1172.

Louis, D.N., Perry, A., Reifenberger, G., VON Deimling, A., Figarella-Branger, D., Cavenee, W.K., Ohgaki, H., Wiestler, O.D., Kleihues, P., Ellison, D.W., 2016. The 2016 World Health Organization classification of tumors of the central nervous system: a summary. Acta Neuropathol. 131, 803–820.

Nakamura, M., Roser, F., Michel, J., Jacobs, C., Samii, M., 2003. The natural history of incidental meningiomas. Neurosurgery 53, 62–70 (discussion 70-1).

Nakamura, M., Roser, F., Michel, J., Jacobs, C., Samii, M., 2005. Volumetric analysis of the growth rate of incompletely resected intracranial meningiomas. Zentralbl. Neurochir. 66, 17–23.

Nakasu, S., Nakasu, Y., Fukami, T., Jito, J., Nozaki, K., 2011. Growth curve analysis of asymptomatic and symptomatic meningiomas. J. Neuro-Oncol. 102, 303–310.

Nydal, R., Lövseth, K., 1965. Distribution of radiocarbon from nuclear tests. Nature 206, 1029–1031.

Olar, A., Wani, K.M., Sulman, E.P., Mansouri, A., Zadeh, G., Wilson, C.D., Demonte, F., Fuller, G.N., Aldape, K.D., 2015. Mitotic index is an independent predictor of recurrence-free survival in meningioma. Brain Pathol. 25, 266–275.

Riemenschneider, M.J., Perry, A., Reifenberger, G., 2006. Histological classification and molecular genetics of meningiomas. Lancet Neurol. 5, 1045–1054.

Roser, F., Nakamura, M., Bellinzona, M., Rosahl, S.K., Ostertag, H., Samii, M., 2004. The prognostic value of progesterone receptor status in meningiomas. J. Clin. Pathol. 57, 1033–1037.

Salehpour, M., Hakansson, K., Possnert, G., 2013. Accelerator mass spectrometry of ultra-small samples with applications in the biosciences. Nucl. Instrum. & Methods in Phys. Res. Sec. B 294, 97–103.

Salehpour, M., Hakansson, K., Possnert, G., 2015. Small sample accelerator mass spectrometry for biomedical applications. Nucl. Instrum. & Methods in Phys. Res. Sec. B 361, 43–47.

Sen, A.K., Srivastava, M.S., 1990. Regression Analysis: Theory. Methods and Applications, Springer-Verlag Berlin Heidelberg.

Siegers, H.P., Zuber, P., Hamou, M.F., VAN Melle, G.D., DE Tribolet, N., 1989. The implications of the heterogeneous distribution of Ki-67 labelled cells in meningiomas. Br. J. Neurosurg. 3, 101–107.

Spalding, K., Bhardwaj, R.D., Buchholz, B., Druid, H., Frisén, J., 2005. Retrospective birth dating of cells in humans. Cell 122, 133–143.

Spalding, K., Arner, E., Westermark, P., Bernard, S., Buchholz, B., Bergmann, O., Blomqvist, L., Hoffstedt, J., Näslund, E., Britton, T., Concha, H., Hassan, M., Rydén, M., Frisén, J., Arner, P., 2008. Dynamics of fat cell turnover in humans. Nature 453, 783–787.

Spalding, K.L., Bergmann, O., Alkass, K., Bernard, S., Salehpour, M., Huttner, H.B., Bostrom, E., Westerlund, I., Vial, C., Buchholz, B.A., Possnert, G., Mash, D.C., Druid, H., Frisen, J., 2013. Dynamics of hippocampal neurogenesis in adult humans. Cell 153, 1219–1227.

Vranic, A., Popovic, M., Cor, A., Prestor, B., Pizem, J., 2010. Mitotic count, brain invasion, and location are independent predictors of recurrence-free survival in primary atypical and malignant meningiomas: a study of 86 patients. Neurosurgery 67, 1124–1132.

Whittle, I.R., Smith, C., Navoo, P., Collie, D., 2004. Meningiomas. Lancet 363, 1535–1543.

Wiemels, J., Wrensch, M., Claus, E.B., 2010. Epidemiology and etiology of meningioma. J. Neuro-Oncol. 99, 307–314.

Yeung, M.S., Zdunek, S., Bergmann, O., Bernard, S., Salehpour, M., Alkass, K., Perl, S., Tisdale, J., Possnert, G., Brundin, L., Druid, H., Frisen, J., 2014. Dynamics of oligodendrocyte generation and myelination in the human brain. Cell 159, 766–774.